Biotechnological production of sialylated solid lipid microparticles as inhibitors of influenza A virus infection

Emeline Richard, Aurélien Traversier, Thomas Julien, Manuel Rosa-Calatrava, Jean-Luc Putaux, Isabelle Jeacomine, Eric Samain

Biotechnological production of sialylated solid lipid microparticles as inhibitors of influenza A virus infection

Emeline Richard[1,*], Aurélien Traversier[2,3], Thomas Julien[2,3], Manuel Rosa-Calatrava[2,3], Jean-Luc Putaux[1], Isabelle Jeacomine[1], Eric Samain[1]

[1] *Univ. Grenoble Alpes, CNRS, CERMAV, F-38000 Grenoble, France*

[2] *CIRI, Centre International de Recherche en Infectiologie, (Team VirPath), Univ Lyon, Inserm, U1111, Université Claude Bernard Lyon 1, CNRS, UMR5308, ENS de Lyon, F-69007 Lyon, France*

[3] *VirNext, Faculté de Médecine RTH Laennec, Université Claude Bernard Lyon 1, Université de Lyon, F-69008 Lyon, France*

* Corresponding author: emeline.richard@cermav.cnrs.fr

Published in: **Glycobiology** *32* (2022), 949-961

DOI: 10.1093/glycob/cwac054

Abstract

Influenza viruses bind to their target through a multivalent interaction of their hemagglutinins (HAs) with sialosides at the host cell surface. To fight the virus, one therapeutic approach consists in developing sialylated multivalent structures that can saturate the virus HAs and prevent the binding to host cells. We describe herein the biotechnological production of sialylated solid lipid microparticles (SSLMs) in three steps: (i) a microbiological step leading to the large-scale production of sialylated maltodextrins by metabolic engineering of an *Escherichia coli* strain, (ii) a new *in vitro* glycosylation process using the amylomaltase MalQ, based on the transglycosylation of the terminal sialoside ligand of the sialylated maltodextrin onto a long-chain alkyl glucoside, and (iii) the formulation of the final SSLMs presenting a multivalent sialic acid. We also describe the morphology and structure of the SSLMs and demonstrate their very promising properties as influenza virus inhibitors using hemagglutination inhibition and microneutralization assays on the human A/H1N1 pdm09 virus.

Introduction

Influenza A viruses (IAVs) are highly contagious pathogens that cause annual epidemics and pandemics in the human population (Salomon and Webster 2009). The infection cycle of IAV is initiated when the viral hemagglutinin (HA) glycoprotein interacts with complex sialoside structures present on the glycoproteins and glycolipids on the surface of the host cells (Karakus et al. 2020; De Vries et al. 2020). This attachment process is based on multivalent bonds to gain stability and prevent the dissociation of viruses (Zhang et al. 2020).

Neuraminidase inhibitors (NAIs) are antivirals recommended worldwide against influenza infection (e.g. oseltamivir and zanamivir; Zhang et al. 2020). They target the viral protein NA, which cleaves the terminal sialic acid from glycan structures for the release of progeny viruses, thereby spreading the virus from the infected host cell to uninfected surrounding cells. However, NAIs have serious side effects and their efficiency has recently come under debate because their use over the past decades has led to the emergence of circulating strains harboring NA mutations (Pan et al. 2013; Abed and Boivin 2017), conferring resistance to these drugs (Hussain et al. 2017). Importantly, the more recent FDA-approved baloxavir antiviral targeting the viral polymerase (Ison et al. 2021), although not yet widely used, will probably suffer the same limitations, because baloxavir-resistant strains harboring specific mutations in the polymerase are already circulating (Hayden et al. 2018; Omoto et al. 2018).

One of the alternative methods of blocking the influenza virus infection is to inhibit virus adhesion by saturating the host HA binding sites with synthetic sialoside ligands. However, the binding energy between a single HA-sialoside ligand pair is too weak to allow the use of a monovalent sialoside as a successful drug candidate. Because of the cluster glycoside effect (Lundquist and Toone 2002), much better binding is observed between HA and multivalent structures that display many copies of specific sialoside ligands. A variety of synthetic multivalent sialoside inhibitors of influenza virus adhesion has already been developed, that includes liposomes (Kingery-Wood et al. 1992), dendrimers (Reuter et al. 1999), synthetic polymers (Sigal et al. 1996; Gambaryan et al. 2005), polysaccharides (Li et al. 2011), and nanoparticles (Papp et al. 2010).

However, the large-scale synthesis of these multivalent sialoside structures represents a double technological challenge, which may explain why this approach has not yet resulted in the development and FDA approval of efficient sialoside-based antiviral drugs against influenza infection.

The first challenge is the synthesis of the sialosides. The avian IAVs virus preferentially binds to sialic acid α(2,3)-linked to galactose, but human-adapted influenza preferentially binds to sialic acid α(2,6)-linked to galactose. The stereoselective synthesis of these sialosides is a notoriously difficult problem in carbohydrate chemistry, resulting in very low yields and high synthesis costs. An efficient alternative is the microbiological approach that has been developed in CERMAV for the production of 3'-sialyllactose (Fierfort and Samain 2008) and 6'-sialyllactose (Drouillard et al. 2010). This technology is based on the expression of specific recombinant sialyltransferase genes in *Escherichia coli* strains that have been genetically engineered to overproduce the cytidine monophosphate-*N*-acetylneuraminic acid (CMP-NeuAc) sugar nucleotide used in the sialylation reaction. These engineered recombinant strains are cultivated at high cell density in the presence of lactose which is internalized and sialylated in the cell to produce sialyllactose at a very high yield.

The second challenge is the multivalent display of the sialoside on a macromolecular multivalent architecture. Many chemical methods have been developed to conjugate carbohydrate structures to various multivalent structures. Among the most effective ones, click-chemistry reactions – which are highly selective and proceed under smooth conditions – have emerged as very powerful techniques for the efficient coupling of functionalized oligosaccharides to complementary activated scaffolds (He et al. 2016). Even though this sophisticated chemistry is easy to perform with high yields at the laboratory scale, the large-scale production and availability of the functionalized oligosaccharides (azide or propargyl sialoside) still hamper the practical development of new drugs based on these technologies.

In the present article, we describe an alternative global biotechnological approach for the large-scale production of sialylated solid lipid microparticles (SSLMs) that shows efficient *in vitro* antiviral action against the A/H1N1 pdm09 influenza virus. As described in **Figure 1**, this approach combines a microbial step for the efficient production of sialylated maltodextrin chains with a new glycosylation method allowing the enzymatic transfer of the terminal sialoside ligand of the sialylated maltodextrin onto a long-chain alkyl glucoside. The resulting amphiphilic structures can then be used to construct SSLMs whose surface is covered with sialoside ligands.

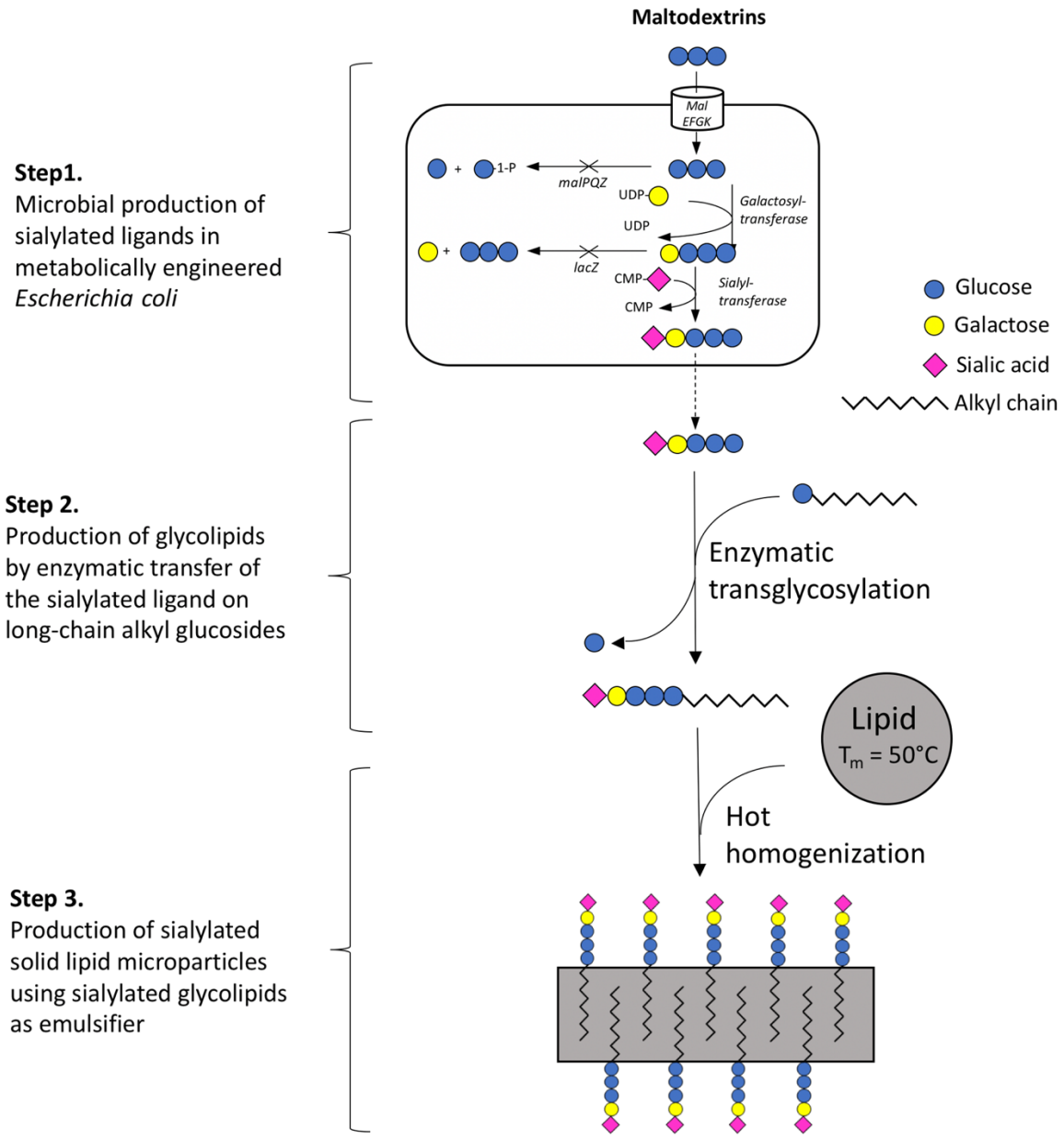

Figure 1. Overall process for the biotechnological preparation of SSLMs. Genes encoding the enzymes are shown in italics.

Table 1. Composition, particle size and structure of bulk materials and sialylated solid lipid microparticles (SSLMs). D-values correspond to the lattice and lamellar spacings deduced from the position of the peaks in the WAXS and SAXS profiles, respectively. "n.d.": not determined.

Reference	Lipid core	Glycoside		Particle size (DLS)		Structure	
		Structure	C (mM)	Average size (nm)	Polydispersity index	d_{WAXS} (nm)	d_{SAXS} (nm)
Cetyl alcohol	-	-	-	-	-	0.36 / 0.40 / 0.43	3.72
Stearyl alcohol	-	-	-	-	-	0.36 / 0.40 / 0.43	4.13
Cetyl palmitate	-	-	-	-	-	0.37 / 0.41	4.25
C12-M5-S	-	C12-M5-S	-	-	-	amorphous	4.07
C16-M5-S	-	C16-M5-S	-			amorphous	4.21
CP*	Cetyl alcohol	-	-	-	-	0.36 / 0.41	4.49
SP*	Stearyl alcohol	-	-	-	-	0.36 / 0.41	4.13 / 5.00
CP1	Cetyl alcohol	C12-M5-S	1	360	0.13	0.36 / 0.41	4.52
CP2	Cetyl alcohol	C16-M5-S	1	332	0.11	0.36 / 0.41	4.52
CP3	Cetyl alcohol	C16-M5-S	0.5	328	0.16	n.d.	n.d.
CP4	Cetyl alcohol	C16-M5-S	0.25	290	0.14	n.d.	n.d.
CP5	Cetyl alcohol	C16-M5-S	0.125	333	0.20	0.36 / 0.41	4.51
SP1	Stearyl alcohol	C16-M5-S	1	221	0.19	0.36 / 0.41	4.13 / 5.00
PP1	Cetyl palmitate	C16-M5-S	1	343	0.24	0.37 / 0.41	4.27
TP1	Tristearin	C12-M5-S	1	422	2.66	n.d.	n.d.

* control samples prepared using the same protocol as for SSLMs, but in the absence of glycosides (**Figures S6** and **S7**).

Results and discussion

Microbial production of sialylated maltodextrins

The strategy for the microbiological production of sialylated maltodextrin is similar to that of our previously described process of sialyllactose synthesis (Fierfort and Samain 2008), except that maltotetraose (M4) was used as the acceptor here instead of lactose. The production strain MQZ-2 is a derivative of the *E. coli* K12 strain DH1 containing null mutations in the following genes: *lacZ*, *nanKETA*, *lacA*, *malPQ*, and *malZ*. The MQZ-2 strain also expresses the heterologous *neuABC* genes from *Campylobacter jejuni*, *lgtE* from *Neisseria meningitis*, and the gene encoding 6ST from *Photobacterium* sp. JT-ISH-224. The MQZ-2 strain was cultivated at high cell density in the presence of an enzymatic starch hydrolysate mainly composed of M4. M4 was actively internalized by the maltose/maltodextrin transport system and accumulated in the cytoplasm due to the inactivation of the *malPQ* and *malZ* genes involved in intracellular catabolism of maltodextrins (Boos and Shuman 1998). A galactose residue was then added on the terminal glucose of the M4 internalized by β(1,4)-galactosyltransferase (encoded by *lgtE*), creating a terminal lactosyl motif which the α(2,6)-sialyltransferase subsequently used as an acceptor to produce an oligosaccharide structure (M4-S) composed of a M4 chain at the reducing end and a sialyllactoside motif at the non-reducing end. At the end of the culture, thin-layer chromatography (TLC) analysis (butanol:formic acid:water; 4:8:1) showed that M4 had been totally converted into a longer oligosaccharide, which migrated as the expected structure Neu5Acα2-6Galβ1-4Glcα1-4Glcα1-4Glcα1-4Glc (M4-S). The mass spectrometry analysis of the crude extract of MQZ-2 (**Figure 2**) confirmed the presence of this structure, showing a main peak at m/z 1168 corresponding to the quasi-molecular ions [M-H]- derived from M4-S. The mass spectrum also showed the presence of a minor peak at m/z 956 and at m/z 795 resulting from the glycosylation of small amounts of maltotriose and maltose initially present in the M4 preparation: M3-S and M2-S, respectively.

Enzymatic transfer of sialoside ligands on long-chain alkyl glucosides

Amylomaltase MalQ (4-α-glucanotransferase; EC 2.4.1.25) is a transglycosidase that catalyzes the glucan transfer from one α(1,4)-glucan to another α(1,4)-glucan or to glucose. The smallest donor substrate recognized by amylomaltase is maltotriose (Palmer et al. 1976). Acting on maltotriose, it releases glucose from the reducing end, forms a maltosyl-enzyme complex, and transfers the maltosyl residue onto the nonreducing end of an acceptor. Using longer

maltodextrin as donor, the amylomaltase MalQ is also able to release maltose or longer maltodextrin (Weiss et al. 2015). The natural acceptors of MalQ are glucose, maltose or any larger maltodextrin. Interestingly, MalQ can also recognize a large variety of α- or β-glucosides as acceptors (Kitahata et al. 1989). The terminal α(1,4)-glucan chain of the M4-S sialoside should be long enough to be recognized as a substrate donor by the amylomaltase MalQ, which may thus be able to release one glucose or maltose from the reducing end of the sialoside and transfer the remaining sialoside chain onto a glucoside acceptor. Using a long-chain alkyl glucoside as the acceptor, this process could provide easy access to the synthesis of sialylated glycosides. To test this possibility, a crude M4-S extract from strain MQZ-2 was incubated with MalQ in the presence of n-dodecyl-β-D-maltoside (C12-M2) as the acceptor. To displace the equilibrium to favor the formation of the desired transglycosylated products, the reaction was conducted in the presence of a glucose oxidase-catalase mixture (Megazyme E-GOXCA) to consume glucose as soon as it was formed. The reaction was conducted with an excess of M4-S, and the TLC analysis showed that C12-M2 disappeared, being correlated with the consumption of M4-S and the formation of a series of glycosides that migrated slower than C12-M2. The reaction was stopped after the total consumption of C12-M2, and the transglycosylation products were purified using reverse phase chromatography. Mass spectrometry revealed a series of amphiphilic sialosides ranging from C12-M4-S to C12-M7-S (**Figure 3A**). The major peak at *m/z* 1448 corresponds to the C12-M5-S structure and NMR spectroscopy indicated that the average degree of polymerization (DP) of the maltodextrin chain was 5.0 monomer units (**Figure S1**). The glycoside structure was unambiguously confirmed by NMR spectroscopy. In the ^{1}H NMR spectrum, the presence of Neu5Ac was indicated by its axial and equatorial H3 signals at d = 1.80 and 2.77 ppm, respectively. Moreover, the C6 signal of the Gal unit is shifted downfield from 60.94 ppm in the free form to 63.71 ppm, which thus confirms the establishment of a glycosidic linkage at this position. The presence of the alkyl chain is proven by the characteristic signals between 0.93 and 1.68 ppm in the ^{1}H NMR spectrum, and between 13.51 and 31.25 ppm in the ^{13}C NMR spectrum (**Table S1**).

The formation of C12-M5-S as the major product, and C12-M4-S is consistent with the expected transglycosylation reaction of M4-S with C12-M2 as the acceptor and the liberation of one glucose or maltose respectively (**Figure 4 (1,2)**). The formation of C12-M6-S and C12-M7-S is more complex and can be explained by a series of transglycosylation reactions and the fact that the liberated M2 can then be used as an acceptor in another disproportionation reaction with M4-S resulting in the formation of M5-S and glucose (**Figure 4 (3)**). Finally, a third transglycosylation reaction would explain the formation of C12-M6-S from M5-S and C12-M2

(**Figure 4 (6)**). Similarly, M5-S can react with C12-M2 to produce C12-M4-S with the formation of maltotriose (M3) (**Figure 4 (4)**) which can itself react with M4-S to form M6-S and glucose (**Figure 4 (5)**) and explain the formation of C12-M7-S by the transglycosylation of this M6-S and C12-M2 (**Figure 4 (7)**).

To produce sialylated glycosides with a longer lipid chain, a transglycosylation reaction was conducted with cetearyl-glucoside (Tego Care CG90 from Evonik) as the acceptor. Cetearyl-glucoside is a mixture of hexadecyl and octadecyl glucoside, which is commercially used as an emulsifier for cosmetic applications. Because CG90 is poorly soluble in water, it was added in a large excess in the transglycosylation reaction. Sialylated glycosides were separated from unreacted alkyl glucoside using reverse phase chromatography, and mass spectrometry revealed a series of amphiphilic sialosides ranging from C16-M3-S to C16-M7-S (**Figure 3B**). No peak originating from C18 glycosides was detected, indicating that only the hexadecyl glucoside fraction of the CG90 had successfully been used as the acceptor and that octadecyl glucose was probably not soluble enough in water to serve as the acceptor. Similar to the C12 series, the main product of the C16 series was centered on C16-M5-S. NMR spectroscopy unambiguously confirmed the glycoside structure (**Table S2**).

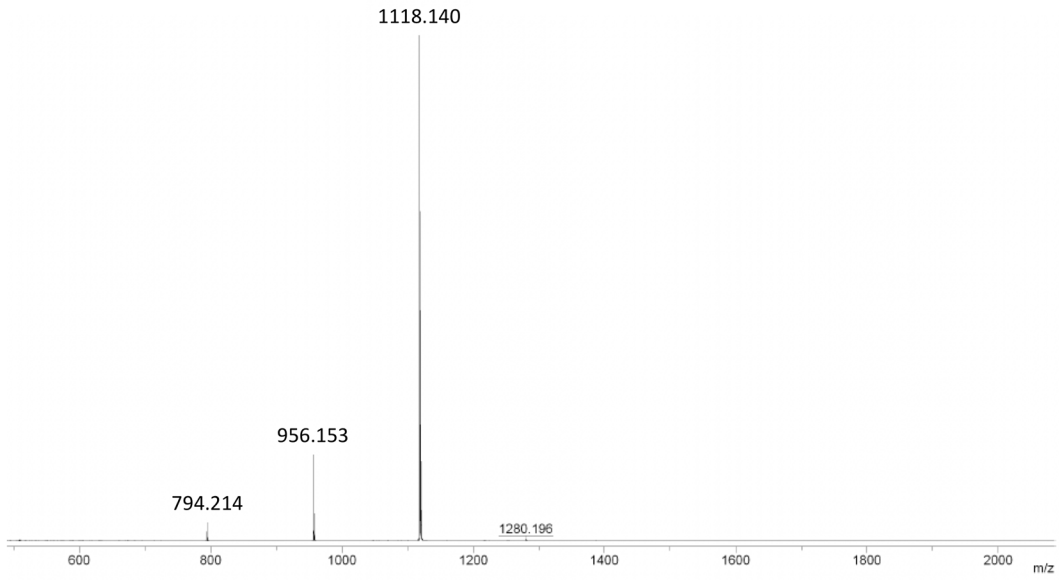

Figure 2. MALDI-TOF mass spectrum in negative mode of the crude extract of MQZ-2. Peaks at m/z 1118, 956, 794 correspond to the quasi-molecular ions [M-H]- derived from sialylated maltotetraose (M4-S), sialylated maltotriose (M3-S) and sialylated maltose (M2-S), respectively.

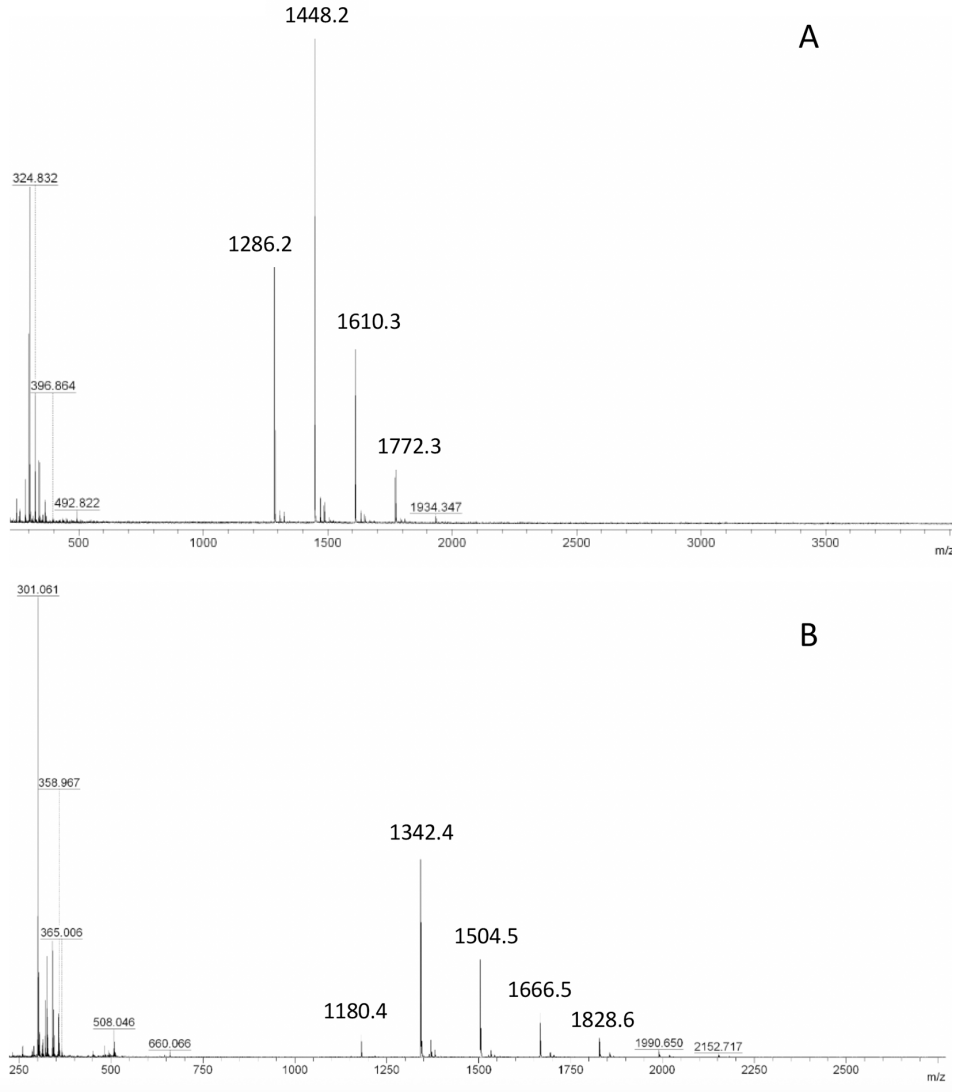

Figure 3. MALDI-TOF mass spectrum in negative mode of the glycoside fraction purified from the transglycosylation reaction mixture of M4-S in the presence of: A) dodecyl β-D-maltoside (C12-M2) or B) cetearyl-glucoside (C16-M1). Peaks at m/z 1286, 1448, 1610, 1772 correspond to the quasi-molecular ions [M-H]- derived from amphiphilic sialosides C12-M4-S, C12-M5-S, C12-M6-S, C12-M7-S. Peak at m/z 1180, 1342, 1504, 1666 and 1828 correspond to the quasi-molecular ions [M-H]- derived from amphiphilic sialosides C16-M3-S, C16-M4-S, C16-M5-S, C16-M6-S, C16-M7-S.

Preparation and characterization of sialylated solid lipid microparticles (SSLMs)

SSLMs were prepared using the hot homogenization technique (Naseri et al. 2015) with hexadecan-1-ol (cetyl alcohol), hexadecyl hexadecanoate (cetyl palmitate), octadecan-1-ol (stearyl alcohol), and propane-1,2,3-triyl trioctadecanoate (tristearin) as the core lipid fraction. All these lipids were solid at physiological temperature with melting temperatures of 49.3, 50, 59.8, and 55 °C, respectively. An oil-in-water microemulsion was prepared at high temperature with ultrasonication of the melted core lipids in the presence of sialylated glycosides.

Immediately after ultrasonication, the microemulsion was quenched to 4 °C, resulting in the crystallization of the core lipid and the formation of a stable aqueous suspension of SSLMs. To estimate the amount of glycosides incorporated in the SSLMs, the microparticles were dialyzed and the concentrated filtrate was analyzed by TLC. The absence of glycosides in this fraction proved their total incorporation into the SSLMs when they were used at 1 mM or below.

When cetyl alcohol was used as the core lipid, the particle size analysis showed that SSLMs prepared with C12-M5-S (CP1) and C16-M5-S (CP2) at 1 mM had a similar average size of around 350 nm with a narrow polydispersity index (PI) below 0.13. After 90 days, the average size of CP1 increased from to 360 to 433, whereas the average size of CP2 increased from 332 to 387. The increase in PI was higher for CP1 (PI = 0.37) than for CP2 (PI = 0.19), indicating that SSLMs prepared with C16-M5-S were more stable than those prepared with C12-M5-S. As shown in **Table 1**, the concentration of C16-M5-S could decrease to 0.5 mM (CP3), 0.25 mM (CP4), and 0.125 mM (CP5) without affecting the stability of the SSLMs or significantly modifying their average size and PI.

Three other lipids were tested as lipid cores of SSLMs constructed with C16-M5-S as the emulsifier. SSLMs prepared with cetylpalmitate (PP1) and stearyl alcohol (SP1) were both stable, with PIs of 0.19 and 0.24, respectively. In contrast, the use of tristearin (TP1) resulted in the formation of unstable SSLMs with a high PI of 2.66.

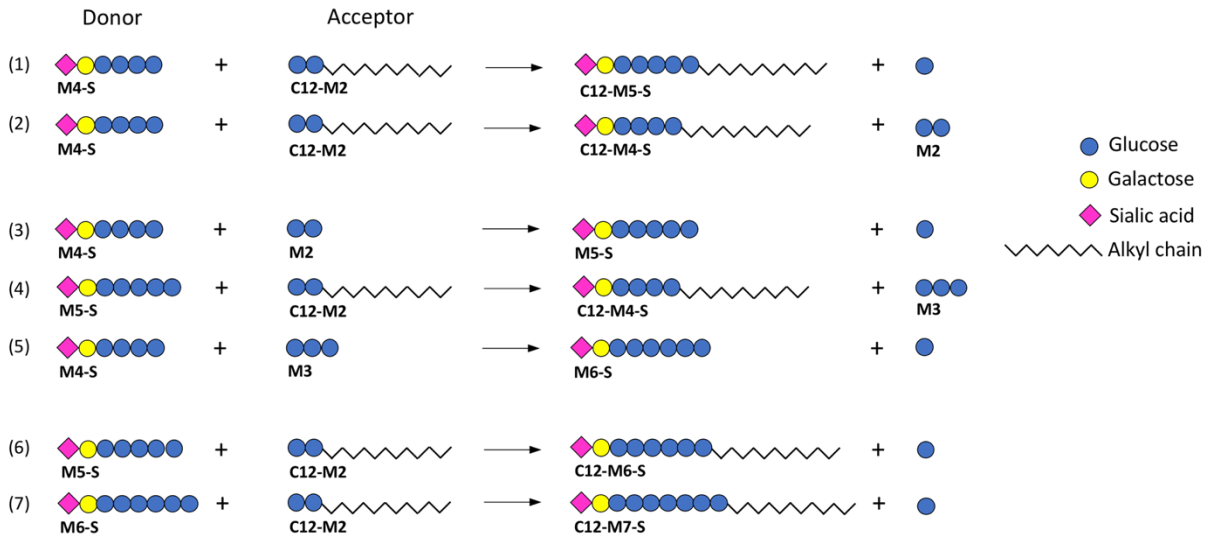

Figure 4. Schematic representation of possible transglycosylation series catalyzed by MalQ, starting with M4-S as donor and C12-M2 as acceptor.

SSLM morphology

Typical transmission electron microscopy (TEM) images of negatively stained preparations of different types of SSLMs are shown in **Figure 5**. The two examples of particles prepared from cetyl alcohol differ in the nature and concentration of the glycoside used in the formulation. CP1 was prepared in the presence of 1 mM C12-M5-S. The SSLMs are flat disks with a roundish shape, although some of them are slightly polygonal (**Figure 5A**). Their diameter ranges between 10 nm and 1 μm. The smallest particles were sometimes lying on their edge, making it possible to measure their thickness (50-300 nm). The shape of the CP5 particles, prepared with 0.125 M C16-M5-S, was more clearly defined. They were mostly flat truncated parallelepipeds with lengths ranging from 300 nm to 1.5 μm, widths from 200 to 700 nm and thicknesses from 50 to 120 nm (**Figure 5B**). The lateral faces seemed to be perpendicular to the supporting carbon film and the angles between the longer faces were about 68 and 112°. The SP1 sample, prepared from stearyl alcohol and 1 mM C16-M5-S, seemed to contain several populations (**Figure 5C**). One population contained nearly perfect and truncated parallelepipeds that were smaller than those in CP5 (length: 50-700 nm; width: 150-400 nm, thickness: 40-80 nm). The angles between the faces were the same as those in CP5. As seen in **Figure S5**, when the particle is oriented edge-on, it was sometimes possible to observe a regular lamellar organization, with the lamellae lying parallel to the large surface. Another type of particle was visible, although it seemed thinner and with less defined roundish shapes. PP1 also contained different types of particles. The largest ones were polydisperse bulky spheroids with diameters ranging from 100 to 700 nm (**Figure 5D**). A second fraction of smaller particles was observed. They were flat, slightly polygonal, their diameters ranging from 20 to 110 nm and thicknesses from 20 to 40 nm.

The Z-average mean value calculated using a dynamic light scattering (DLS) analysis was based on a sphere with a diffusion coefficient equal to that of the scattering particle. Considering that the particles were flat in most systems, the equivalent spheres had a smaller diameter. Nevertheless, the relative average sizes measured using DLS were in fairly good agreement with those observed from the TEM images.

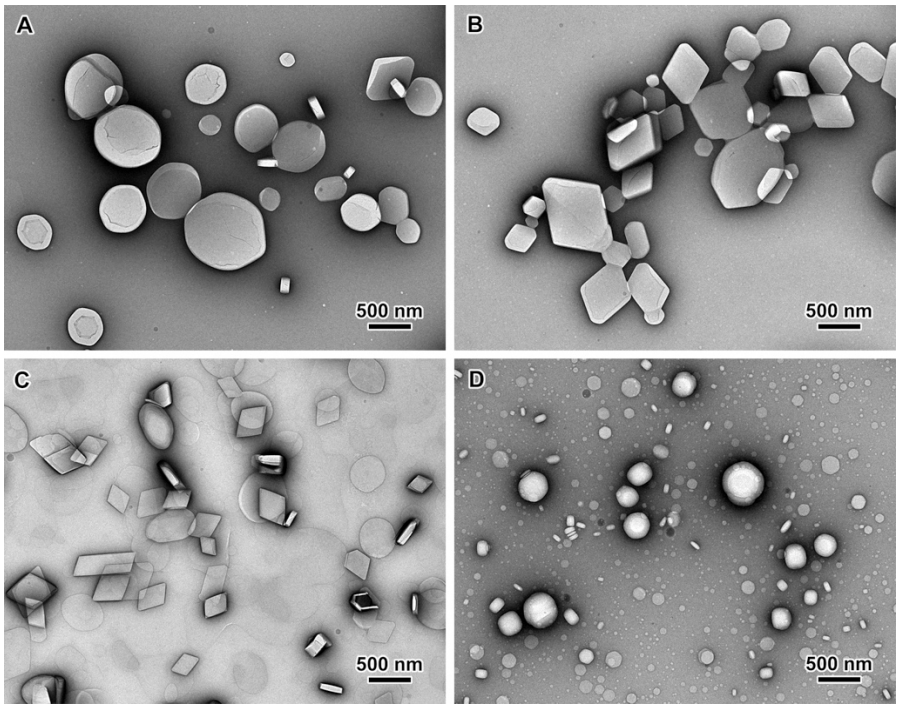

Figure 5. TEM images of negatively stained preparations of particles from CP1 (a), CP5 (b), SP1 (c) and PP1 (d) formulations (**Table 1**).

Structure of bulk compounds and SSLMs

The crystal structure of the samples was determined using small- and wide-angle X-ray scattering (SAXS and WAXS) analyses (**Figure 6**) by plotting the scattered intensity as a function of the scattering vector $q = 2\pi/d$, where d is the repeat distance between the corresponding lattice planes. The SAXS profile of bulk cetyl alcohol showed a series of equidistant peaks, the first one located at $q_1 = 1.69$ nm^{-1}, and the second and third ones at $q_2 = 2q_1$ and $q_3 = 3q_1$ (**Figure 6A**). This profile suggests a regular lamellar organization with a repeat distance of $d_{lam} = 2\pi/q_1 = 3.71$ nm. The chains in the stearyl alcohol crystal were organized in a similar fashion, but considering the longer fatty moiety, the stronger peak in the SAXS profile was located at $q_1 = 1.52$ nm^{-1} (**Figure 6A**), corresponding to a lamellar repeat of $d_{lam} = 4.13$ nm. For cetyl palmitate, the stronger peak was found at $q_1 = 1.47$ nm^{-1}, for a lamellar repeat $d_{lam} = 4.25$ nm. Within the 14-19 nm^{-1} q-region, the WAXS profiles of bulk cetyl alcohol and stearyl alcohol were identical and exhibited three main peaks at 14.77, 15.57, and 17.62 nm^{-1}, corresponding to lattice distances of 0.43, 0.40, and 0.36 nm, respectively. The profile of cetyl palmitate contained two main peaks at 15.26 and 16.93 nm^{-1}, corresponding to lattice distances of 0.41 and 0.37 nm, respectively (**Figure 6B**). These results show that both bulk cetyl alcohol and stearyl alcohol are crystallized in the monoclinic γ allomorph, in agreement

with previous studies. They have both a bilayer organization in which the cetyl alcohol and stearyl alcohol molecules are tilted by about 58° with respect to the lamellar plane (Abrahamsson et al. 1960; Métivaud et al. 2005; Berwanger et al. 2009). Cetyl palmitate appears to be crystallized in the β-form that also corresponds to a monoclinic unit cell (Métivaud et al. 2005), sometimes considered as orthorhombic, because the angle of the molecules to the lamellar plane is nearly 90° (Lukowski et al. 2000).

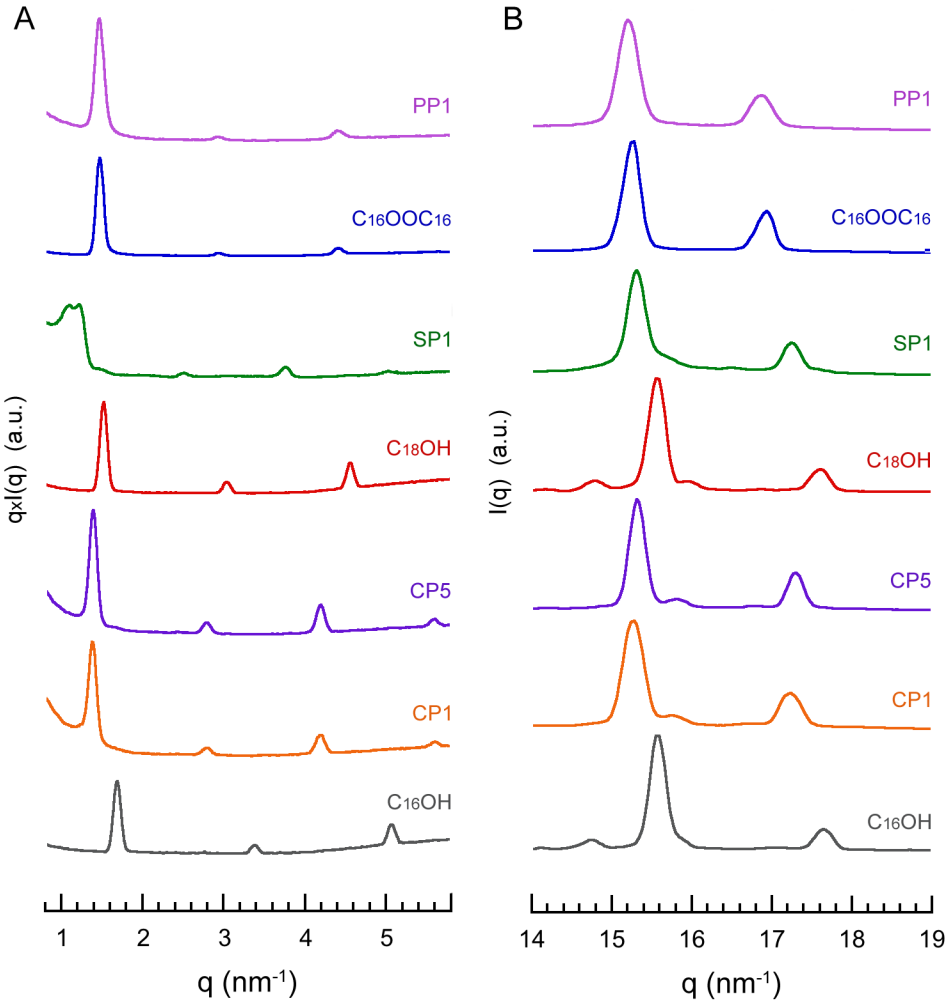

Figure 6. q×I(q) SAXS (A) and WAXS (B) profiles of bulk compounds and SSLMs. The reference of each sample is given in **Table 1**.

The crystal structures of the SSLMs prepared from cetyl alcohol or stearyl alcohol were similar, but they differed from those of the parent bulk compounds. The WAXS profiles of CP1, CP2 (not shown), CP5, and SP1 exhibited two main peaks at q = 15.32 and 17.30 nm^{-1} and a weaker one at 15.82 nm^{-1} (**Figure 6B**), corresponding to lattice spacings of 0.41, 0.36, and 0.40 nm, respectively. The structure of the PP1 particles was similar to that of the parent bulk cetyl

palmitate (**Figure 6B**). The SAXS profiles of SSLMs were also typical of bilayer organizations with lamellar repeats of d_{lam} = 4.52 nm (q_1 = 1.39 nm^{-1}) for CP1, CP2, and CP5, larger than that of the parent bulk cetyl alcohol (**Figure 6A**). The lamellar repeat of PP1 particles (q_1 = 1.47 nm^{-1}, d_{lam} = 4.27 nm) was nearly identical to that of bulk cetyl palmitate. The peaks detected in the profile of SP1 can be divided into two subsets, each associated with a lamellar structure: a major one with d_{lam} = 5.08 nm (q_1 = 1.23 nm^{-1}) and a minor one with d_{lam} = 4.13 nm (q_1 = 1.52 nm^{-1}). The peak positions of the minor phase corresponded to those of the γ-phase of bulk stearyl alcohol (**Figure 6A**). The crystal structures of the SSLMs prepared from cetyl alcohol and stearyl alcohol thus differed from those of the parent bulk compounds. The data from CP1, CP2, CP5, and the major form of SP1 are consistent with an orthorhombic β allomorph, in agreement with the TEM images in which the vertical surfaces of the particles seemed to be perpendicular to the supporting carbon film (**Figure 5A-C** and Supporting Material **Figure S5**). From the X-ray scattering data only, it is not possible to determine if the two phases detected in the SP1 sample coexist in each particle or correspond to two different fractions, although the latter possibility seems to be supported by the variety of particle shapes observed in TEM images (**Figure 5C**).

Additional control experiments were carried out in order to shed some light on the origin of the structural differences between the bulk *n*-fatty alcohols and the corresponding SSLMs. First, two samples of bulk cetyl alcohol were heated to 100 °C. One was allowed to cool down slowly to room temperature, while the other was quench-frozen in ice-cooled water. In both cases, the WAXS profiles were identical to that of bulk cetyl alcohol (**Figure S6Ba-c**). However, the SAXS profile of the quench-frozen specimen contained two subsets of equidistant peaks (**Figure S6Ac**): a major one corresponding to that of bulk cetyl alcohol (**Figure S6Aa**) and a minor one to that of CP5 SSLMs (**Figure S6Ae**). In another experiment, particles were prepared from cetyl alcohol following the same protocol as for SSLMs, but without adding the glycoside. Cetyl alcohol was thus heated, sonicated and quench-frozen (sample referred to as CP in **Table 1**). On the one hand, the WAXS profile was identical to that of CP5, prepared in the presence of glycoside (**Figure S6Bd**). On the other hand, the SAXS profile contained two subsets of equidistant peaks, but this time, the major one was the same as that of CP5, while the minor one corresponded to that of bulk cetyl alcohol (**Figure S6Ad**). Similar observations were noted for particles prepared from stearyl alcohol without adding the glycoside (sample referred to as SP in **Table 1**). The SAXS and WAXS profiles were the same as those of the SP1 SSLMs (**Figures S7Bb,c** and **S7Ab,c**, respectively), including the presence of a minor fraction exhibiting the peak positions of bulk stearyl alcohol (**Figure S7Aa**). These results show that

the β-form of SSLMs can be obtained without glycosides present in the formulation. It is a minor fraction when the bulk compound is melted and quench-frozen, but the major form when the melted compound is dispersed in water into microdroplets under strong sonication before being quench-frozen. The high surface-to-volume ratio of the droplets may induce a confinement effect, promoting the nucleation and growth of the metastable β phase upon fast-freezing. Homogenization/fragmentation of the melted cetyl alcohol and stearyl alcohol by sonication and quench-freezing are thus both important aspects of the protocols, influencing not only the size of the SSLMs, but also their final crystal structure. Long-chain *n*-fatty alcohols with an even number of carbons have been reported to crystallize in the γ-form, but those with an odd number crystallize in the β-form (Precht 1976; Ventolá et al. 2002). The fact that CPn and SP1 SSLMs crystallized into the β-form, but their parent fatty alcohols corresponded to the γ allomorph is consistent with the previous observation that a metastable β-phase can be obtained by quenching stearyl alcohol from the melt and that this phase has the same structure as the β-phase of the odd fatty alcohols (Ventolá et al. 2002).

Evaluation of SSLMs as inhibitors of influenza A virus

The potential antiviral action of different SSLMs on the human A/H1N1 pdm09 virus was evaluated with standard hemagglutination inhibition (HI) and microneutralization (MN) assays (Truelove et al. 2016). The HI assay utilizes the natural process of HA-induced hemagglutination of the red blood cells; in contrast, the MN assay measures cytopathic effects of the infectious virus through plaque formation (Hayden and Palese 2016). These processes are blocked when sufficient amounts of compounds (antibody, decoy) with affinity to the virus particle – especially hemagglutinin – are present. Serum from mice immunized with commercial TIV Vaxigrip and PBS were used as positive and negative controls, respectively for HI and MN assays.

The results presented in **Table 2** show that the most promising compound is CP2, which contains 1 mM of C16-M5-S as the sialylated glycoside. Interestingly, this compound harbored a significant capacity to inhibit both virus HA-inducing hemagglutination of red blood cells (HI titer: 512) and virus infection of Madin-Darby canine kidney (MDCK) cells (MN titer, 640). In contrast, CP1, which contains 1 mM of C12-M5-S as the sialylated glycoside, harbored lower activity, suggesting the importance of the size of the lipid chain. CP3, CP4, and CP5 compounds, which contain lower amounts of C16-M5-S, were less active (HI titers: < 256 or 128, MN titers: 40 or 160) indicating that a minimal surface density of sialylated ligand is required for efficient virus binding. The SP1compound, which contains a different lipid core

(stearyl alcohol instead of cetyl alcohol in CP1), showed a high capacity to inhibit virus HA-inducing hemagglutination (HI titer: 1024), but lower inhibition was observed in the MN assay (MN titer: 80). Although these results are not completely consistent, the SP1 compound is also a promising candidate that could be further evaluated with CP2 and other compounds in *in vitro* and optionally in *in vivo* potency assays.

Of note, the PP1 compound showed a high cytotoxicity for red blood cells; therefore, a minimal dilution of 8192 was necessary. At this very low concentration, we did not observe any capacity to inhibit virus HA-induced hemagglutination of red blood cells and its cytotoxicity was too high to test the compound with a MN assay. This toxicity may be related to a difference in the crystalline structure of the particles between active CP2 and SP1, which contain simple aliphatic alcohol as the lipid core and the cytotoxic PP1 in which the lipid core is an ester containing two lipid chains. In this respect, compound TP1, which contains tristearin, was too unstable to be tested further.

Table 2. Evaluation of antiviral properties of SSLMs by standard hemagglutination inhibition (HI) and microneutralization (MN) assays. The hemagglutination inhibition (HI) titer was designated as the inverse of the highest dilution at which detectable HI activity was still present. The microneutralization (MN) titer was designated as the inverse of the highest dilution at which no CPE was observed in at least 2 wells over 4. Serums from mice immunized with commercial TIV Vaxigrip and PBS were used as controls for HI and MN assays.

Reference	Virus titer	
	HI[a]	MN[b]
PBS (Ctrl –)	<2	<20
C12-M5-S	<8	NT[c]
C16-M5-S	<256	<20
CP1	<256	80
CP2	512	640
CP3	<256	160
CP4	<256	40
CP5	<128	40
PP1	<8192	NT
SP1	1024	80
TP1	NT	NT
Serum (Ctrl +)	128	160

[a] HI: hemagglutination inhibition of red blood cells
[b] Microneutralization: infection inhibition of Madin-Darby canine kidney (MDCK) cells
[c] Not tested

Conclusion

Antivirals play a major role in the treatment and control of influenza epidemics and pandemics. Neuraminidase and polymerase inhibitors have demonstrated clinical benefits, but the emergence of viral resistance may cripple the current arsenal, particularly in a context in which the vaccine options are not optimal either. In this study, we explored an alternative way of blocking the influenza virus infection based on SSLMs. Classically, solid lipid microparticles (SLMs) are used as drug carrier for prolonging the drug release, preventing its degradation and improving its bioavailability. SLMs also present the advantages of being biocompatible and productible at large industrial scale (Gugu et al. 2015; Scalia et al. 2015). Few articles describe the use of decorated solid lipid nanoparticles (SLNs) for drug delivery on a selective target (Garanti et al. 2020; Sandri et al. 2010; Hu et al. 2017). To the best of our knowledge, this work describes the first synthesis of decorated SLMs for multivalent display and not for drug vectorization. Indeed, these SSLMs can act as a decoy mimicking the natural epithelium surface. Eventually, formulated in a nasal spray, SSLMs could be a promising new antiviral drug, able to inhibit virus adhesion by saturating the host HA binding sites.

These SSLMs made of sialosides with a C16 alkyl chain are produced using a unique biotechnological approach that provides for their large-scale production at a reasonable cost. The first microbial production step of sialylated maltodextrins chains is easily scalable to very large quantities, as is the production of human milk oligosaccharides. Interestingly, the enzymatic synthesis of alkyl-sialosides can be carried out in the crude cellular extract without requiring a prior purification of either the sialylated maltodextrins or amylomaltase. Likewise, due to their highly amphiphilic nature, the resulting alkyl-sialosides can be directly purified in one step from the crude reaction mixture using reverse phase chromatography. The final step of SSLM preparation is a self-assembling process which is straightforward to implement.

Other advantages of the process include the very low cost of the raw materials (maltodextrins, alkylglucosides, and lipids) and the composition of the final SSLMs formed by the assembly of natural molecules (glucose, galactose, sialic acid, and lipid) attached by common biochemical glycosidic linkages. Given this natural composition, the SSLMs are likely nontoxic and fully biodegradable.

Our results indicate that SSLMs are promising antiviral candidates because they have shown significant inhibition action against A/H1N1 pdm09 influenza virus in HI and in MN *in vitro* assays. These results pave the way for further evaluation of SSLMs against other influenza A subtypes and influenza B strains to characterize their putative broad-spectrum antiviral

activity against influenza viruses. In addition, other physiological *in vitro* models, e.g. human reconstructed airway epithelium for example, and *in vivo* models of infection, e.g. mouse or ferret, must be used to confirm the potential of SSLMs as inhibitors of influenza viruses.

This overall approach can also be adapted to the synthesis of other glycosylated solid lipid microparticles containing different sialosides such as α(2,3)-linked sialosides, which are recognized by avian influenza viruses.

Materials and methods

Plasmids and strains

The host strain MQZ was constructed by disrupting the *malPQ* and *malZ* genes in the strain ZLKA (Fierfort and Samain 2008) which was a *lacZ*, *lacA* and *nanKETA* null mutant derived from the *E. coli* strain DH1 (DSM 4235).

To knockout the *malP* and *malQ* genes, a 3.110 kb segment located between nucleotides 371 of *malP* and 1097 of *malQ* was deleted and replaced by the 5'TCTAG sequence as follows: two DNA segments flanking the deleted sequence were amplified by PCR. The upstream 1.080 kb segment was amplified with primers 5'-GTCGACtcgactcaatggcaactgtc and 5'-TCTAGAgtggggtaataccgttggtg and the downstream 0.958 kb segment was amplified with primers 5'-TCTAGaatgccgattggcttgtatc and 5'-GGATCCtctgtccaaatccttcagca. The two amplified fragments were ligated at their terminal *Xba*I restriction site and cloned together into the *Bam*HI *Sal*I sites of the suicide vector pKO3. The deletion was then carried out according to the pKO3 gene replacement protocol in Link et al. (1997).

To knockout the *malZ* gene, a 0.491 kb segment located between nucleotides 594 and 1084 of *malZ* was deleted as follows: two DNA segments flanking the deleted sequence were amplified by PCR. The upstream 0.847 kb segment was amplified with primers 5'-GGATCCGCGTATCTCGCTGTATGTCGGTTTC and 5'-GGATCCGCGTATCTCGCTGTATGTCGGTTTC and the downstream 0.843 kb segment was amplified with primers 5'-AAGCTTGATCACCGAAGCGGCGAAAGAAAC and 5'-GTCGACGATTTAGACGCTCATTATGACGCCCTC. The two amplified fragments were ligated at their terminal *Hind*III restriction site and cloned together into the *Bam*HI *Sal*I sites of the suicide vector pKO3. The deletion was then carried out according to the pKO3 gene replacement protocol in Link et al. (1997).

The sialoside production strain MQZ-2 was constructed by transforming the host strain MQZ with the three plasmids, pBS-SS, pSU-6ST and pBBR3-lgtEm. Plasmid pBS-SS was a

pBluescript derivative containing the *neuABC* genes from *C. jejuni* ATCC 43438 encoding CMP-Neu5Ac synthetase, sialic acid synthase and GlcNAc-6-phosphate 2 epimerase, respectively (Drouillard et al. 2010). Plasmid pSU-6ST was a pSU2718 derivative carrying the *Photobacterium* sp. JT-ISH-224 gene for α(2,6)-sialyltransferase (Richard et al. 2017). Plasmid pBBR3-lgtEm containing the *N. meningitis lgtE* gene for β1,4 galactosyltransferase was constructed as follows: a 0.942 kb DNA fragment containing the sequence of *lgtE* (GenBank: AAB48387.1) was amplified by PCR using the genomic DNA of *N. meningitis* 126E as a template. An *Xba*I site was added to the left primer (5'-TCTAGATACCGGGGCTATTGAAACC) and a *Sac*I site was added to the right primer (GAGCTCGCGGGAATGACAGTGTATC). The amplified fragment was first cloned into pCR4Blunt-TOPO vector (Invitrogen) and then subcloned into the *Xba*I and *Sac*I sites of plasmid pBBR1-MCS3 plasmid (Kovach et al. 1995) to form pBBR3-lgtEm.

To clone the amylomaltase *malQ* gene, a 2.090 kb DNA fragment containing the *malQ* sequence was amplified by PCR using the genomic DNA of *E. coli* K12 as a template and the following primers: 5'-CCATGGAAAGCAAACGTCTGGATAATG and 5'-ACTCTACTTCTTCTTCGCTGCAG. The amplified fragment was first cloned into pCR4Blunt-TOPO vector (Invitrogen) and then sub-cloned into the *Nco*I and *Eco*RI sites of expression vector pProEX-HTb (Invitrogen) to form pPro-malQ. For the production of recombinant MalQ, the strain MS was transformed with pPro-malQ plasmid and cultivated in a 3-L bioreactor containing 1.5 L of Terrific broth at 30 °C. MalQ production was induced by adding IPTG (150 $mg.L^{-1}$) when the optical density of the culture reached 5.0. Cells were harvested by centrifugation 4 h after induction and the cell pellet was resuspended in 150 mL of potassium phosphate buffer (10 mM, pH 7.0). Cells were disrupted in a high-pressure cell homogenizer (Constant System Ltd) and the crude extract containing 25 $units.mL^{-1}$ of MalQ was aliquoted and frozen at -80 °C until its use as a direct MalQ source in enzymatic synthetic reactions. MalQ activity was determined by measuring the initial rate of glucose formation from maltotriose using a glucose enzymatic assay kit from Megazyme. One MalQ unit was defined as the amount of enzyme required to produce 1 $\mu mol.min^{-1}$ of glucose from maltotriose at 25 °C.

Preparation of M4

The strain of *Pseudomonas stutzeri* NRRL B-3389 was obtained from the DSMZ collection (DSM 13627) and cultured on starch for the production of maltotetraose-producing amylase as described in Robyt and Ackerman (1971). After cell removal by centrifugation, 100 mL of the

culture supernatant was filtered-sterilized through a 0.22 µm filter and added to 1 L of a 100 $g.L^{-1}$ autoclaved gelatinized starch solution. After 48 h of incubation at 30 °C, TLC analysis (butanol:formic acid:water; 4:8:1) confirmed the M4 formation as the major starch hydrolysis product and indicated the presence of small amount of maltose and maltotriose. The mixture was centrifuged and the M4-containing supernatant was autoclaved and kept at room temperature prior to its use as an acceptor for the synthesis of M4-ligands.

Production of sialylated maltodextrins

Strain MQZ-2 was cultured at high cell density as previously described (Priem et al. 2002) in a 3-L reactor containing 1.5 L of mineral culture medium in presence of ampicillin (100 $mg.L^{-1}$), tetracycline (20 $mg.L^{-1}$) and/or chloramphenicol (50 $mg.L^{-1}$). The culture consisted of three phases: an exponential growth phase, starting with the inoculation of the bioreactor and lasting until exhaustion of the carbon substrate (glucose 17.5 $g.L^{-1}$), a 5 h fed-batch phase with a high glycerol feeding rate of 5 $g.L^{-1}.h^{-1}$, and a 25-h fed-batch phase with a lower glycerol feeding rate of 3 $g.L^{-1}.h^{-1}$. Maltotetraose (10 g, 6.7 $g.L^{-1}$) and the inducer (IPTG, 50 $mg.L^{-1}$) were added at the end of the exponential phase. At the end of the culture, bacterial cells were recovered by centrifugation (7000 × *g*, 20 min) and the pellet was resuspended in the same volume of distilled water (2 L). The cells were permeabilized by heating to 100 °C for 45 min and after cooling, the pH was lowered to 4.0 with HCl. After another centrifugation step (7000 × *g* for 20 min), the supernatant containing the sialoside was recovered and the pH was adjusted to 7.0 with NaOH. The M4-S concentration of the crude intracellular fraction obtained was determined using a glucose assay. After acid hydrolysis (4 h in 1 N HCl), the glucose rate was determined using the glucose enzymatic kit from Megazyme at 3 $g.L^{-1}$, therefore, the concentration of the sialoside was 5 $g.L^{-1}$.

Production of sialylated glycosides

Dodecyl β-D-maltoside (C12-M2) and cetearyl glucoside were obtained from Carbosynth (DD06199) and from Evonik (Tego Care CG90), respectively. The glucose oxidase/catalase mixture was purchased from Megazyme (E-GOXCA).

For the production of C12 glycosides, C12-M2 (1 g, 1.96 mmol) was solubilized in 600 mL of intracellular fraction from the MQZ-2 culture containing M4-S (3 g, 2.68 mmol). MalQ (150 units), glucose oxidase (1200 units), and catalase (30,000 units) were added and the mixture was incubated at room temperature. The reaction was followed by TLC analysis

(butanol:acetic acid:water; 2:1:1) and stopped after 24 h (total consumption of dodecyl-maltose) by heating to 100 °C for 20 min to inactivate the enzymes. After 20 min of centrifugation at 9000 rpm, the supernatant was loaded on a C18-column (10 g Reverlis) at 5 mL.min^{-1}. The column was washed with 100 mL of deionized water and the desired product was eluted with 500 mL of a methanol gradient from 0 to 100% at 5 mL.min^{-1}. The elution was followed by TLC analysis (butanol:acetic acid:water; 2:1:1). After freeze-drying, 870 mg of purified sialylated glycosides was obtained (yield: 30%).

For the production of C16- glycosides, cetearyl-glucoside (CG90) (2 g) was solubilized in large excess, in 400 mL of the intracellular fraction from the MQZ-2 culture containing M4-S (2 g, 1.79 mmol). MalQ (200 units), glucose oxidase (1200 units), and catalase (30000 units) were added and the mixture was incubated at 30 °C for better glycoside solubilization. The reaction was followed by TLC and stopped after 48 h (total consumption of M4-S) by heating at 100 °C for 20 min to inactivate the enzymes. Purification followed the same steps as for the C12 glycoside, and 510 mg of purified sialylated glycosides were obtained (yield: 20%).

DEPTQ and proton NMR spectra were recorded with a Bruker Avance 400 spectrometer operating at a frequency of 100.618 MHz for ^{13}C and 400.13 MHz for ^{1}H. Samples were solubilized in D_2O at a temperature of 25 °C. Residual signal of the solvent was used as the internal standard: HOD at 4.8 ppm. DEPTQ spectra were recorded using 90 pulses, 20,161 Hz spectral width, 65,536 data points, 1.62 s acquisition time, 2 s relaxation delay, and 20,480 scans. Proton spectra were recorded with a 4000 Hz spectral width, 65,536 data points, 8.19 s acquisition times, 10 s relaxation delays, and 16 to 64 scans. The ^{1}H and ^{13}C-NMR assignments were based on ^{1}H-^{1}H homonuclear and ^{1}H-^{13}C heteronuclear correlation experiments (correlation spectroscopy, COSY; heteronuclear multiple-bond correlation, HMBC; heteronuclear single quantum correlation, HSQC). They were performed with a 4000 Hz spectral width, 2048 data points, 0.255 s acquisition time, 1 to 1.5 s relaxation delay; 40 to 512 scans were accumulated.

Preparation of sialylated solid lipid microparticles

The solid lipids (135 mg in 10 mL) were melted at 100 °C in the presence of either C12-M5-S or C16-M5-S. Unless otherwise indicated in the text, the glycoside concentration was 1 mM. The mixture was dispersed by vortexing and then sonicated (Labsonic, Stedim) at 60 W for 5 min at 90 °C. The oil-in-water emulsion was then immediately poured in a pre-chilled 125 mL sterile Erlenmeyer flask pre-chilled in an ice bath. To estimate the amount of incorporated

glycosides, the SSLMs were dialyzed against water (MWCO: 12–14 kDa, ZelluTrans, 24 h). The concentrated filtrate and retentate were analyzed by TLC (butanol:acetic acid:water; 2:1:1).

Dynamic light scattering

SSLMs were analyzed with regard to particle size and size distribution using DLS. The mean particle size and the polydispersity index (PI) were obtained using a Zetasizer Nano ZS (Malvern Instruments, Malvern, United Kingdom). Samples were diluted 100 times with water before analysis to yield a suitable scattering intensity. The Z-average mean size and PIs were obtained by calculating the average of three measurements in 10 mm diameter disposable plastic cells.

Transmission electron microscopy

Drops of dilute aqueous SSLM suspensions were deposited on glow-discharged carbon-coated copper grids and negatively stained with 2 wt% uranyl acetate. The preparations were observed in a JEOL JEM-2100 Plus microscope operating at 200 kV and images were recorded with a Gatan Rio 16 digital camera.

WAXS and SAXS

Powders of lyophilized SSLMs were poured into 1-mm outer diameter glass capillaries that were flame-sealed and X-rayed with Ni-filtered CuKα radiation ($\lambda = 0.1542$ nm) under vacuum in a Warhus chamber. Two-dimensional scattering patterns were recorded on Fujifilm imaging plates, and read off-line with a Fujifilm BAS 1800-II bioimaging analyzer. The capillary-to-detector distance was set to about 4.5 and 16.5 cm to collect WAXS and SAXS data, respectively. The precise distance was calibrated using calcite and silver behenate powders, respectively. Scattering profiles were calculated by radially averaging the 2D patterns.

Cells and viruses

Influenza virus A/H1N1 pdm09 (A/Lyon/969/09 H1N1, Centre National de Référence des Virus Respiratoires, Lyon, France Sud) was produced in MDCK (ATCC CCL-34) cells using EMEM supplemented with 2 mM L-glutamine (Sigma Aldrich), penicillin (100 $U.mL^{-1}$), streptomycin (100 $\mu g.mL^{-1}$; Lonza) and 1 $\mu g.mL^{-1}$ trypsin at 37 °C and 5% CO_2. Viral titers in

plaque forming units (PFU.mL^{-1}) and tissue culture infectious dose 50% (50.mL^{-1} TCID) were determined in MDCK cells as previously described (Pizzorno et al. 2019).

HI assay

Potential of HI property of SSLMs was evaluated on chicken red blood cells (RBC) using a standard hemagglutination assay, as described previously (Mandon et al. 2020). SSLMs were serially diluted in phosphate buffered saline (PBS) and 50 µL of RBC was added. After 1 h at room temperature, a dilution of each SSLM was determined as the pre-dilution to avoid cytotoxicity on RBCs. Then SSLMs were pre-diluted as determined previously, and 25 µL of each SSLM was serially diluted in PBS. Then, 25 µL of a virus dilution with 4 hemagglutination units (HAu) was added and the plate was incubated for 1 h at room temperature. To each mixture, 50 µL of 0.5% chicken RBCs were added and incubated for 1 h at room temperature. As previously described in Mandon et al. (2020), serum from mice immunized with commercial TIV Vaxigrip and protecting against an A(H1N1)pdm09 lethal dose infection, and PBS were used as positive and negative controls, respectively. The HI titer was designated as the inverse of the highest dilution at which detectable HI activity was still present.

Microneutralization assay

SSLMs were serially diluted in IM (infection medium as serum-free MEM Eagle with EBSS, Lonza) supplemented with 2 mM L-glutamine (Gibco), penicillin (100 U.mL^{-1}) and streptomycin (100 µg.mL^{-1}; Gibco) and 1µg.mL^{-1} trypsin acetylated from bovine pancreas (Sigma). Serial dilutions were mixed with 100 TCID50 of A/ H1N1 pdm09 virus and incubated at 37 °C for 1 h. Then, 50 µL of the SSLM-virus mixture was added to 150 µL of IM on MDCK cells and incubated at 37 °C and 5% CO_2. After 96 h of incubation, the presence of cytopathic effects (CPE) was controlled under microscopy observation. As previously described in Mandon et al. (2020), serum from mice immunized with commercial TIV Vaxigrip and protecting against an A(H1N1)pdm09 lethal dose infection, and PBS were used as positive and negative controls, respectively. The MN titer was determined as the inverse of the highest dilution at which no CPE were observed in at least 2 out of 4 wells, as previously described (Mandon et al. 2020).

Abbreviations used in this manuscript

CMP-NeuAc, cytidine monophosphate-N-acetylneuraminic acid; CPE, cytopathic effects; Gal, galactose; Glc, glucose; HA, hemagglutinin; DLS, dynamic light scattering; EBSS, Earle's balanced salt solution; EMEM, Eagle's minimum essential medium; HI, hemagglutination inhibition; IAV, influenza virus; IPTG, isopropyl-1-thio-β-D-galactopyranoside; M2, maltose; M4, maltotetraose; M4-S, sialylated maltotetraose; MN, microneutralisation; NA, neuraminidase; NAI, neuraminidase inhibitor; PI, polydispersity index; NeuAc, *N*-acetyl-neuraminic acid; NMR, nuclear magnetic resonance; PBS, phosphate buffer saline; RBC, red blood cell; TEM, transmission electron microscopy; TLC, thin-layer chromatography.

Funding and acknowledgments

This work was supported by the French National Research Agency (ANR) through IDEX "Innovation Grant 2017" (ANR-15-IDEX-0002), LabEx ARCANE and CBH-EUR-GS (ANR-17-EURE-0003), Glyco@Alps (ANR-15-IDEX-02), Institut Carnot PolyNat (CARN-025-01) and SATT Linksium "Projet de maturation Glycoflu". The NanoBio-ICMG Platform (UAR 2607, Grenoble) is acknowledged for providing facilities for mass spectrometry (A. Durand, L. Fort, R. Gueret), NMR spectroscopy and electron microscopy.

References

Abed Y and Boivin G (2017) A review of clinical Influenza A and B infections with reduced susceptibility to both oseltamivir and zanamivir. *Open Forum Infectious Diseases* 4(3): ofx105.

Abrahamsson S, Larsson G and von Sydow E (1960) The crystal structure of the monoclinic form of n-hexadecanol. *Acta Crystallographica* 13(10): 770–774.

Berwanger R, Henschel A, Knorr K, Huber P and Pelster R (2009) Phase transitions and molecular dynamics of n-hexadecanol confined in silicon nanochannels. *Physical Review B - Condensed Matter and Materials Physics* 79(12): 125442.

Boos W and Shuman H (1998) Maltose/Maltodextrin System of Escherichia coli: Transport, metabolism, and regulation. *Microbiology and Molecular Biology Reviews* 62(1): 204–229.

Drouillard S, Mine T, Kajiwara H, Yamamoto T and Samain E (2010) Efficient synthesis of 6'-sialyllactose, 6,6;-disialyllactose, and 6'-KDO-lactose by metabolically engineered E. coli expressing a multifunctional sialyltransferase from the Photobacterium sp. JT-ISH-224. *Carbohydrate Research* 345(10): 1394–1399.

Fierfort N and Samain E (2008) Genetic engineering of Escherichia coli for the economical production of sialylated oligosaccharides. *Journal of Biotechnology* 134(3–4): 261–265.

Gambaryan A, Boravleva E, Matrosovich T, Matrosovich M, Klenk H, Moiseeva E, Tuzikov A, Chinarev A, Pazynina G and Bovin N (2005) Polymer-bound 6 sialyl-N-acetyllactosamine protects mice infected by influenza virus. *Antiviral Research* 68(3): 116–123.

Garanti T, Alhnan MA and Wan KW (2020) RGD-decorated solid lipid nanoparticles

enhance tumor targeting, penetration and anticancer effect of asiatic acid. *Nanomedicine* 15(16): 1567–1583.

Gugu TH, Chime SA and Attama AA (2015) Solid lipid microparticles: An approach for improving oral bioavailability of aspirin. *Asian Journal of Pharmaceutical Sciences* 10(5): 425–432.

Hayden FG, Palese P. Influenza virus. In "Clinical Virology", Richman DD, Whitley RJ, Hayden F Eds., ASM Press, 2016, Chap. 43., pp. 1009-1058.

Hayden FG, Sugaya N, Hirotsu N, Lee N, de Jong MD, Hurt AC, Ishida T, Sekino H, Yamada K, Portsmouth S, Kawaguchi K, Shishido T, Arai M, Tsuchiya K, Uehara T and Watanabe A (2018) Baloxavir Marboxil for Uncomplicated Influenza in Adults and Adolescents. *New England Journal of Medicine* 379(10): 913–923.

He XP, Zeng YL, Zang Y, Li J, Field RA and Chen GR (2016) Carbohydrate CuAAC click chemistry for therapy and diagnosis. *Carbohydrate Research* 429: 1–22.

Hu J-B, Song G-L, Liu D, Li S-J, Wu J-H, Kang X-Q, Qi J, Jin F-Y, Wang X-J, Xu X-L, Ying X-Y, Yu L, You J, Du Y-Z and Hu B (2017) Sialic acid-modified solid lipid nanoparticles as vascular endothelium-targeting carriers for ischemia-reperfusion-induced acute renal injury Sialic acid-modified solid lipid nanoparticles as vascular endothelium-targeting carriers for ischemia-reperfusion-induced acute renal injury. Drug Delivery 24(1): 1856–1867.

Hussain M, Galvin H, Haw TY, Nutsford A and Husain M (2017) Drug resistance in influenza A virus: the epidemiology and management. *Infection and Drug Resistance* 10: 121–134.

Ison MG, Hayden FG, Hay AJ, Gubareva L V., Govorkova EA, Takashita E and McKimm-Breschkin JL (2021) Influenza polymerase inhibitor resistance: Assessment of the current state of the art - A report of the isirv Antiviral group. *Antiviral Research* 194: 105158.

Karakus U, Pohl MO and Stertz S (2020) Breaking the convention: Sialoglycan variants, coreceptors, and alternative receptors for Influenza A virus entry. *Journal of Virology* 94(4).

Kingery-Wood J, Williams KW, Sigal GB and Whitesides GM (1992) The agglutination of erythrocytes by Influenza virus is strongly inhibited by liposomes incorporating an analog of sialyl gangliosides. *Journal of the American Chemical Society* 114(18): 7303–7305.

Kitahata S, Ishikawa H, Miyata T and Tanaka O (1989) Production of rubusoside derivatives by transgalactosylation of various β-galactosidases. *Agricultural and Biological Chemistry* 53(11): 2923–2928.

Kovach ME, Elzer A' PH, Steven Hill D, Robertson GT, Farris MA, Martin R, Ii R, Peterson KM and Peterson KM (1995) Four new derivatives of the broad-host-range cloning vector pBBR1MCS, carrying different antibiotic-resistance cassettes. *Gene* 166: 175–176.

Li X, Wu P, Gao GF and Cheng S (2011) Carbohydrate-functionalized chitosan fiber for influenza virus capture. *Biomacromolecules* 12(11): 3962–3969.

Link AJ, Phillips D and Church GM (1997) Methods for generating precise deletions and insertions in the genome of wild-type Escherichia coli: Application to open reading frame characterization. *Journal of Bacteriology* 179(20): 6228–6237.

Lukowski G, Kasbohm J, Pflegel P, Illing A and Wulff H (2000) Crystallographic investigation of cetylpalmitate solid lipid nanoparticles. *International Journal of Pharmaceutics* 196(2): 201–205.

Lundquist JJ and Toone EJ (2002) The cluster glycoside effect. *Chemical Reviews* 102(2): 555–578.

Mandon ED, Pizzorno A, Traversier A, Champagne A, Hamelin ME, Lina B, Boivin G,

Dejean E, Rosa-Calatrava M and Jawhari A (2020) Novel calixarene-based surfactant enables low dose split inactivated vaccine protection against influenza infection. *Vaccine* 38(2): 278–287.

Métivaud V, Lefèvre A, Ventolà L, Négrier P, Moreno E, Calvet T, Mondieig D and Cuevas-Diarte MA (2005) Hexadecane (C16H34) + 1-Hexadecanol (C 16H33OH) binary system: Crystal structures of the components and experimental phase diagram. application to thermal protection of liquids. *Chemistry of Materials* 17(12): 3302–3310.

Naseri N, Valizadeh H and Zakeri-Milani P (2015) Solid lipid nanoparticles and nanostructured lipid carriers: Structure preparation and application. *Advanced Pharmaceutical Bulletin* 5(3): 305–313.

Omoto S, Speranzini V, Hashimoto T, Noshi T, Yamaguchi H, Kawai M, Kawaguchi K, Uehara T, Shishido T, Naito A and Cusack S (2018) Characterization of influenza virus variants induced by treatment with the endonuclease inhibitor baloxavir marboxil. *Scientific Reports* 8(1): 9633.

Palmer TN, Ryman BE and Whelan WJ (1976) The action pattern of amylomaltase from Escherichia coli. *European Journal of Biochemistry* 69: 105–115.

Pan P, Li L, Li Y, Li D and Hou T (2013) Insights into susceptibility of antiviral drugs against the E119G mutant of 2009 influenza A (H1N1) neuraminidase by molecular dynamics simulations and free energy calculations. *Antiviral Research* 100(2): 356–364.

Papp I, Sieben C, Ludwig K, Roskamp M, Böttcher C, Schlecht S, Herrmann A and Haag R (2010) Inhibition of Influenza virus infection by multivalent sialic-acid-functionalized gold nanoparticles. *Small* 6(24): 2900–2906.

Pizzorno A, Terrier O, de Lamballerie CN, Julien T, Padey B, Traversier A, Roche M, Hamelin ME, Rhéaume C, Croze S, Escuret V, Poissy J, Lina B, Legras-Lachuer C, Textoris J, Boivin G and Rosa-Calatrava M (2019) Repurposing of drugs as novel influenza inhibitors from clinical gene expression infection signatures. *Frontiers in Immunology* 10: 60.

Precht D (1976) Kristallstrukturuntersuchungen an Fettalkoholen und Fettsäuren mit Elektronen- und Röntgenbeugung II. *Fette, Seifen, Anstrichmittel* 78(5): 189–192.

Priem B, Gilbert M, Wakarchuk WW, Heyraud A and Samain E (2002) A new fermentation process allows large-scale production of human milk oligosaccharides by metabolically engineered bacteria. *Glycobiology* 12(4): 235–240.

Reuter JD, Myc A, Hayes MM, Gan Z, Roy R, Qin D, Yin R, Piehler LT, Esfand R, Tomalia DA and Baker JR (1999) Inhibition of viral adhesion and infection by sialic-acid-conjugated dendritic polymers. *Bioconjugate Chemistry* 10(2): 271–278.

Richard E, Pifferi C, Fiore M, Samain E, Le Gouëllec A, Fort S, Renaudet O and Priem B (2017) Chemobacterial synthesis of a sialyl-Tn cyclopeptide vaccine candidate. *ChemBioChem* 18(17): 1730–1734.

Robyt JF and Ackerman RJ (1971) Isolation, purification, and characterization of a maltotetraose-producing Amylase from *Pseudomonas stutzeri*. *Archives of Biochemistry and Biophysics* 145: 105–114.

Salomon R and Webster RG (2009) The influenza virus enigma. *Cell* 136(3): 402–410.

Sandri G, Bonferoni MC, Gkçe EH, Ferrari F, Rossi S, Patrini M and Caramella C (2010) Chitosan-associated SLN: In vitro and ex vivo characterization of cyclosporine A loaded ophthalmic systems. *Journal of Microencapsulation* 27(8): 735–746.

Scalia S, Young PM and Traini D (2015) Solid lipid microparticles as an approach to drug delivery. *Expert Opinion on Drug Delivery* 12(4): 583–599.

Sigal GB, Mammen M, Dahmann G and Whitesides GM (1996) Polyacrylamides bearing pendant α-sialoside groups strongly inhibit agglutination of erythrocytes by influenza virus: The strong inhibition reflects enhanced binding through cooperative polyvalent interactions. *Journal of the American Chemical Society* 118(16): 3789–3800.

Truelove S, Zhu H, Lessler J, Riley S, Read JM, Wang S, Kwok KO, Guan Y, Jiang CQ and Cummings DAT (2016) A comparison of hemagglutination inhibition and neutralization assays for characterizing immunity to seasonal influenza A. *Influenza and other Respiratory Viruses* 10(6): 518–524.

Ventolá L, Ramírez M, Calvet T, Solans X, Cuevas-Diarte MA, Negrier P, Mondieig D, van Miltenburg JC and Oonk HAJ (2002) Polymorphism of N-alkanols: 1-heptadecanol, 1-octadecanol, 1-nonadecanol, and 1-eicosanol. *Chemistry of Materials* 14(2): 508–517.

De Vries E, Du W, Guo H and De Haan CAM (2020) Influenza A virus hemagglutinin-neuraminidase-receptor balance: Preserving virus motility. *Trends in Microbiology* 28: 57–67.

Weiss SC, Skerra A and Schiefner A (2015) Structural basis for the interconversion of maltodextrins by MalQ, the amylomaltase of Escherichia coli. *Journal of Biological Chemistry* 290(35): 21352–21364.

Zhang Q, Liang T, Nandakumar KS and Liu S (2020) Emerging and state of the art hemagglutinin-targeted influenza virus inhibitors. *Expert Opinion on Pharmacotherapy* 22(6): 715–728.

Supplementary Data

Table S1. NMR characterization of C12-M5-S.

C12-M5-S

NeuAc			
		C2	100.33
H3	1.8 (t, $J_{H,H}$=12.32 Hz)	C3	40.30
	2.77 (dd, $J_{2,3}$=$J_{3,4}$=4.98 Hz)		
H4	3.72	C4	68.38
H5	3.92	C5	51.85
H6	3.79	C6	72.58
H7	3.63	C7	68.47
H8	3.90	C8	71.24
H9	3.91 – 3.71	C9	62.74
NHAc : CH3	2.09 (s)	CH3	22.26
		C=O	175
Gal β			
H1	4.48 (d, $J_{1,2}$=7.88 Hz)	C1	103.24
H2	3.60	C2	70.81
H3	3.70	C3	71.80
H4	4.01	C4	73.34
H5	3.86	C5	73.45
H6	4.03 – 3.66	C6	63.62
Glu α			
H1	5.43 (m)	C1	99.69
H2	3.6	C2	71.58
H3	3.93	C3	71.57
H4	3.69	C4	79.6
H5	3.63	C5	74.62
H6	3.89	C6	60.42
Glu β			
H1	4.52 (d, $J_{1,2}$=7.94 Hz)	C1	102.08
H2	3.35 (m)	C2	73.03
H3	3.82	C3	76.31
H4	3.70	C4	77.23
H5	3.72	C5	77.06
H6	3.88	C6	60.70
Aliphatic chain			
C**H3**	0.93 (m)	**C**H3	13.51
C**H2**	1.41 (m)	**C**H2	25.05
C**H2**	1.68 (m)	**C**H2	28.66
C**H2**	1.34	**C**H2	28.78
C**H2**	1.34	**C**H2	31.25
C**H2**	1.34	**C**H2	22.08

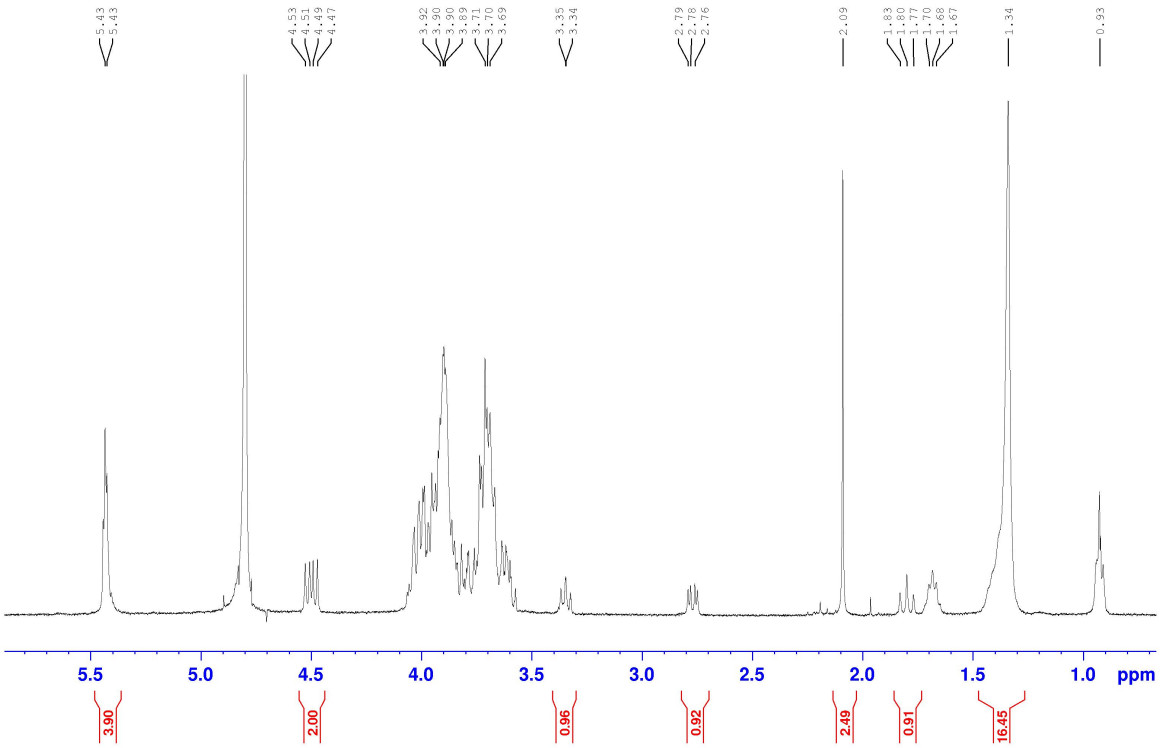

Figure S1. ^{1}H-NMR spectrum of C12-M5-S.

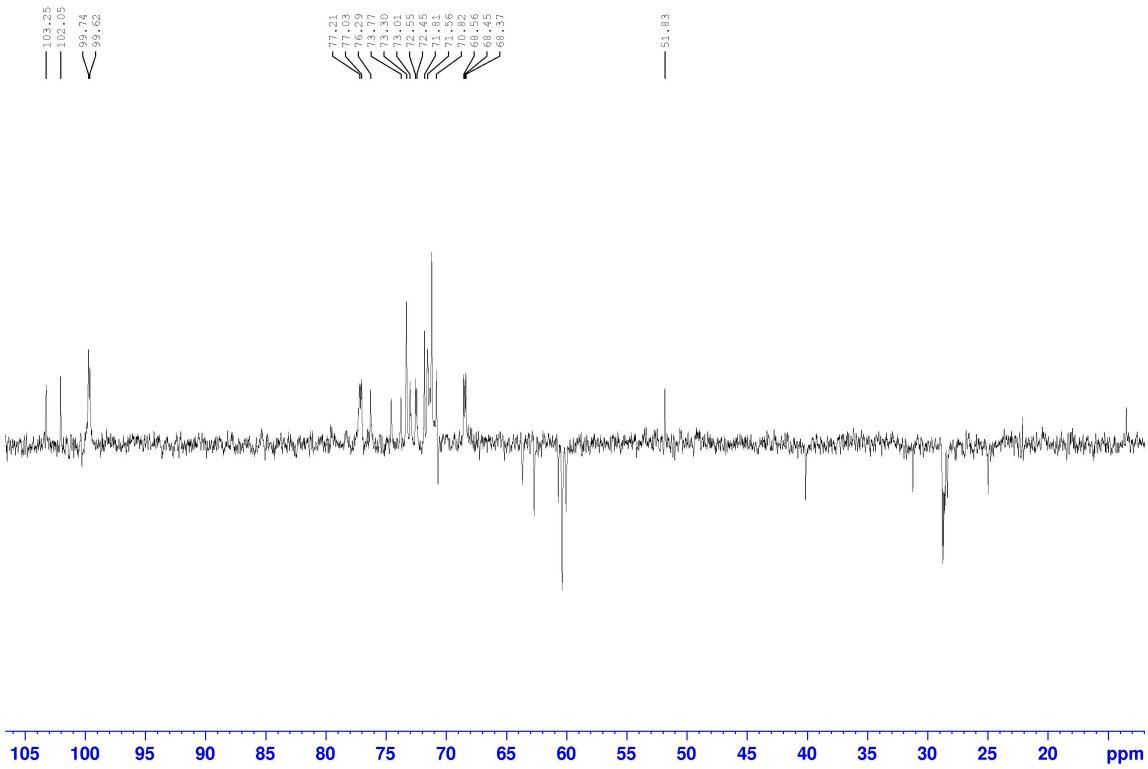

Figure S2. ^{13}C-DEPTQ135-NMR spectrum of C12-M5-S.

Table S2. NMR characterization of glycosides.

C16-M5-S

NeuAc

		C2	100.33
H3	1.77 (t, $J_{H,H}$=11.99 Hz) 2.76 (m)	C3	40.13
H4	3.71	C4	68.43
H5	3.89	C5	51.89
H6	3.74	C6	72.55
H7	3.61	C7	68.42
H8	3.93	C8	71.80
H9	3.93 – 3.69	C9	62.69
NHAc : CH3	2.08 (s)	CH3	22.16
		C=O	174.97
		COOH	173.5

Gal β

H1	4.48 (m)	C1	103.17
H2	3.60	C2	70.86
H3	3.69	C3	72.57
H4	3.98	C4	68.30
H5	3.85	C5	73.70
H6	4.01 – 3.68	C6	63.48

Glu α

H1	5.41 – 5.45 (m,m)	C1	99.27 – 99.6
H2	3.69 – 3.72	C2	71.5 – 71.6
H3	3.88 – 4.00	C3	71.51
H4	3.67 – 3.71	C4	77.1 – 77.4
H5	3.60 – 3.63	C5	71.22 – 71.5
H6	3.91 – 3.85	C6	59.95 – 60.2

Glu α (linked to aliphatic chain)

H1	4.91 (m)	C1	99.59
H2	3.62	C2	71.40
H3	4.01	C3	71.51
H4	3.67	C4	77.10
H5	3.90 – 3.95	C5	71.70
H6	3.76	C6	60.20

Aliphatic chain

C**H3**	0.96 (m)	**C**H3	14.03
C**H2**	1.39 (m)	**C**H2	26.01
C**H2**	1.35 (m)	**C**H2	22.70
C**H2**	1.70 (m)	**C**H2	29.44
C**H2**	1.35 (m)	**C**H2	29.46
C**H2**	1.33 (m)	**C**H2	32.05

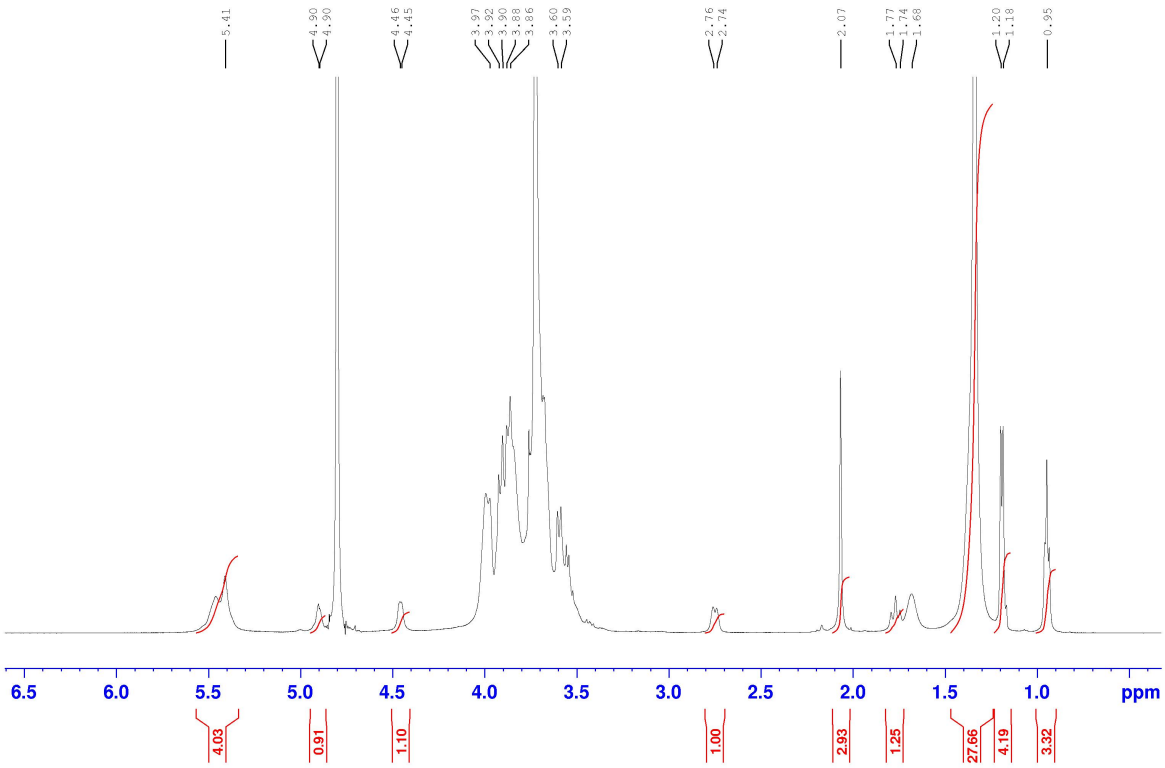

Figure S3. ^{1}H-NMR spectrum of C16-M5-S.

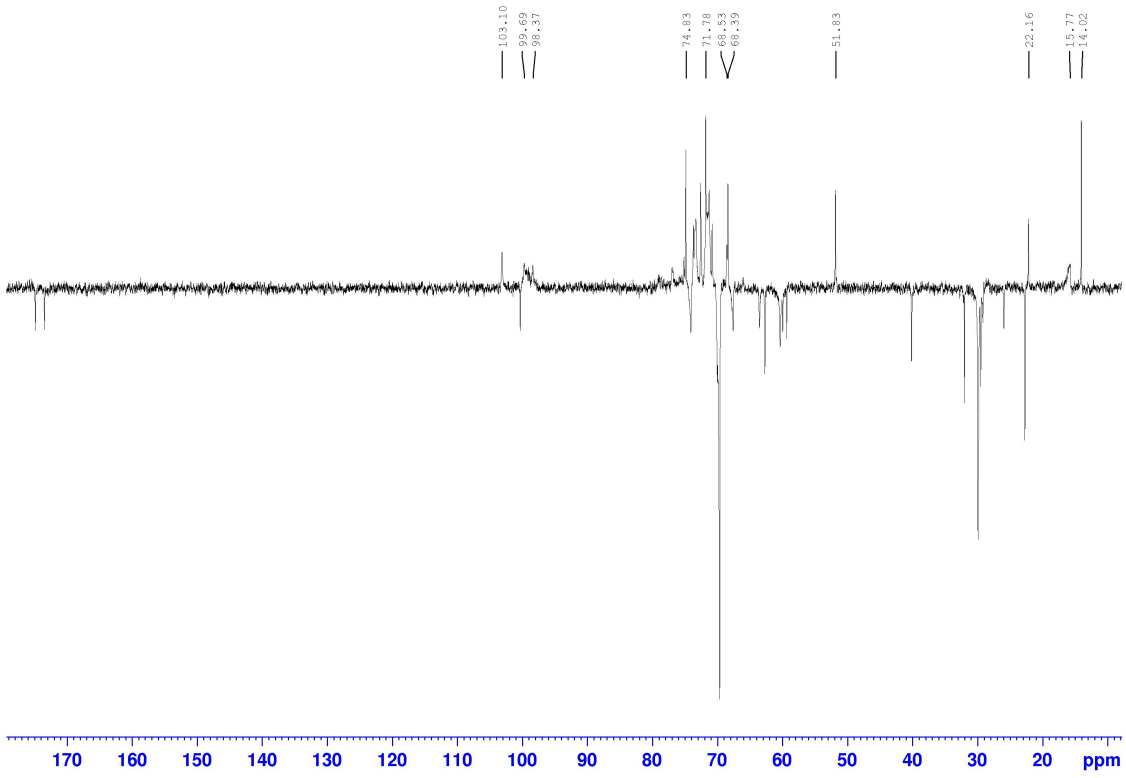

Figure S4. ^{13}C-DEPTQ135-NMR spectrum of C16-M5-S.

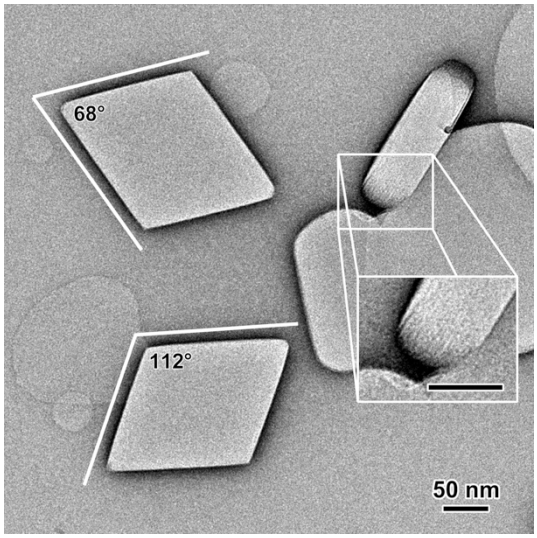

Figure S5. TEM image of negatively stained SP1 particles. In the inset, the particle is seen edge-on and the lamellar structure is visible (bar: 50 nm).

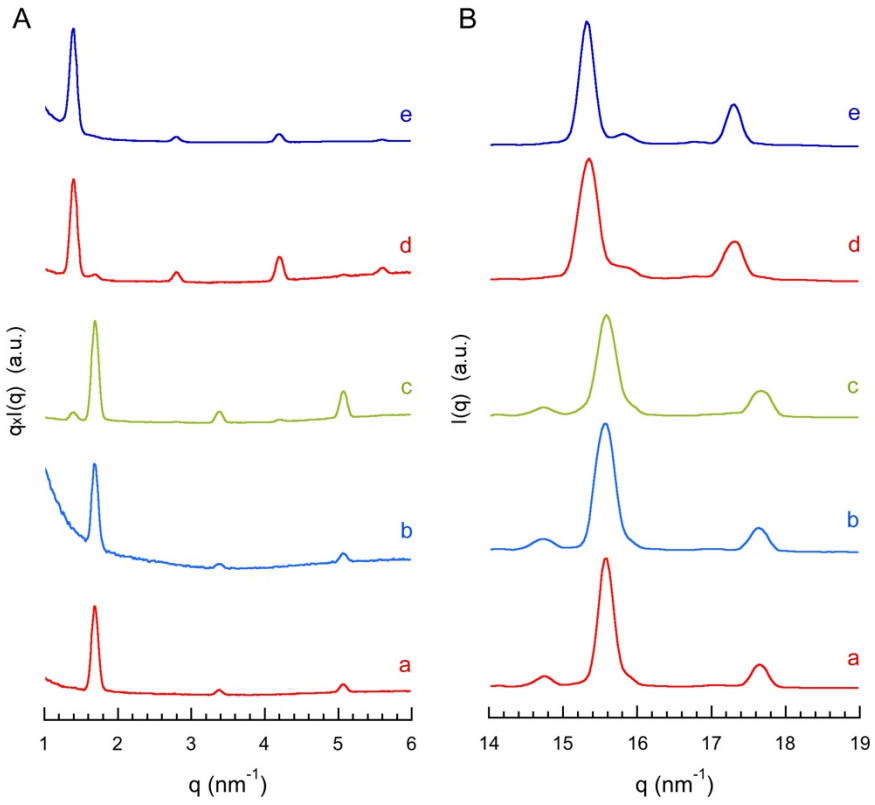

Figure S6. q×I(q) SAXS (A) and WAXS (B) profiles of bulk and SSLM $C_{16}OH$ control samples: a) bulk $C_{16}OH$; b) bulk $C_{16}OH$ heated to 100 °C and cooled down to room temperature; c) bulk $C_{16}OH$ heated to 100 °C and quench-frozen; d) $C_{16}OH$ prepared with the SSLM method but without glycoside (CP in **Table 1**); e) CP5 SSLMs.

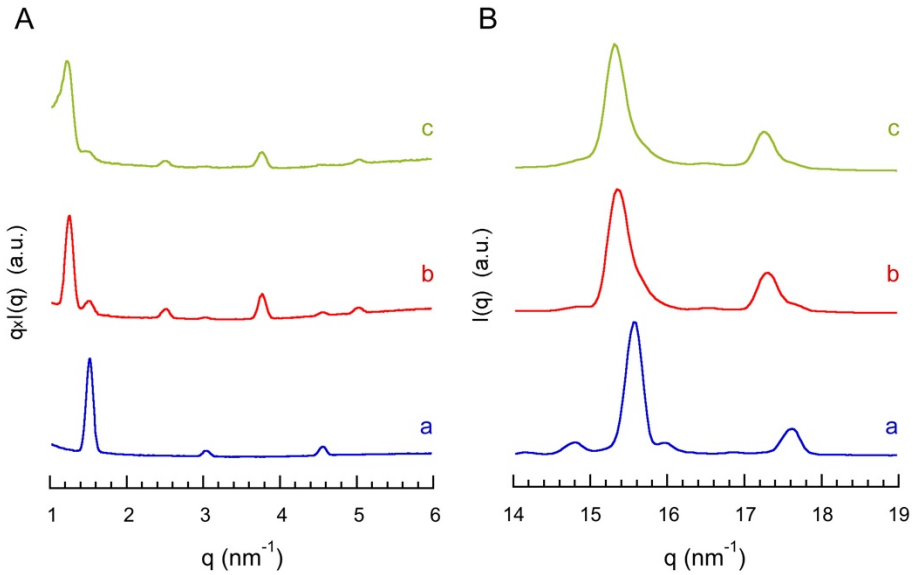

Figure S7. q×I(q) SAXS (A) and WAXS (B) profiles of bulk and SSLM C_{18}OH control samples: a) bulk C_{18}OH; b) C_{18}OH prepared with the SSLM method but without glycoside (SP in **Table 1**); c) SP1 SSLMs.